JOURNAL OF NANO- AND ELECTRONIC PHYSICS
Vol. **8** No 2, 02028(6pp) (2016)

ЖУРНАЛ НАНО- ТА ЕЛЕКТРОННОЇ ФІЗИКИ
Том **8** № 2, 02028(6cc) (2016)

Anodized Nanoporous Titania Thin Films for Dental Application: Structure' Effect on Corrosion Behavior

A. Boucheham[1,2,*], A. Karaali[1], M. Berouaken[2], Y. Larbah[3]

[1] *Laboratoire de Thermodynamique et Traitement de Surfaces des Matériaux, Département de Physique, Faculté des Sciences Exactes, Université de Constantine1, 25000 Constantine, Algeria*
[2] *Centre de Recherche en Technologie des Semi-conducteurs pour l'Energétique, 02, Bd Dr Frantz Fanon, les 07 merveilles, BP: 140, 16038 Algiers, Algeria*
[3] *Materials Technology Department, Physics Faculty, Oran University of Sciences and Technology USTO-MB, BP1505 Oran, Algeria*

(Received 20 February 2016; revised manuscript received 09 June 2016; published online 21 June 2016)

Nanostructured Titania layers formed on the surface of titanium and titanium alloys by anodic oxidation play an important role in the enhancement of their biocompatibility and osseointegration in the human body. For this purpose, we aimed to study in the current work the structural and electrochemical properties of amorphous and crystallized nanostructured TiO_2 thin films elaborated on Ti6Al4V substrate by electrochemical anodization in fluoride ions (F^-) containing electrolyte at 10 V during 15 min and heat treated in air at 550 °C for 2 h. The morphology, chemical composition and phase composition of synthesized layers were investigated using field emission scanning electron microscopy (FE-SEM) and X-ray diffraction (XRD). The corrosion resistance improvement of both as-anodized and annealed titania layers was evaluated in 0.9 wt. % NaCl solution with pH = 6.4 at room temperature by means of open circuit potential (E_{oc}),potentiodynamic polarization (PDYN) and electrochemical impedance spectroscopy (EIS).

Keywords: Titanium alloys, Dental implants, Anodization, Nanoporous TiO_2, Electrochemical impedance spectroscopy.

DOI: 10.21272/jnep.8(2).02028 PACS numbers: 87.85.jj, 82.45.Bb

1. INTRODUCTION

Titanium and its alloys are widely used in orthopaedic and prosthodontic fields as implants to replace damaged bones and hard tissues [1-6] due to its good corrosion resistance, biocompatibility and excellent osseo-integration compared with stainless steel and Co-alloys [7, 8]. Unfortunately, these alloys exhibit often a fail after long-term use in the human body due to an incomplete osseo-integration [9] and ions release. Therefore, to overcome these problems, the modification of the smooth surface of Ti-alloys have received considerable attention in order to improve the biocompatibility of titanium and to enhance the bone growth, this modification was carried out by various coating methods such as: thermal oxidation [10, 11], electrochemical anodization [12-15], hydroxyapatite coating [16-18] and alkaline treatment with NaOH [19, 20], etc.

It was found that the electrochemical anodization in fluoride-containing electrolytes is the simplest and the low cost technique that was employed extensively to synthesis nanoporous and nanotubular TiO_2 thin films on titanium and Ti-based surface alloys [21].

In this work, we focus our study, firstly, on the elaboration of an amorphous nanoporous titania layer on Ti6Al4V alloy by anodic oxidation in aqueous solution containing 0.5 wt. % hydrofluoric acid at 10 V for 15 minutes, secondly, on the effect of the annealing at 550 °C during 2 hours in air on the crystallization of the formed TiO_2 thin film, finally, we investigate and compare the electrochemical properties of the substrate with the as-anodized and annealed titania layers.

2. EXPERIMENTAL PROCEDURE

1.1 Samples Preparation

The samples used in this work are medical grade titanium alloys, grade 5 (Ti6AL4V alloys) with the following chemical composistion (wt. %) of 6.3 Al, 3.9 V, 0.185 O, 0.019 C, 0.18 Fe, 0.011 N, Ti balance as evaluated with energy dispersive X-ray spectroscopy (EDS) device attached to the SEM.

Prior to the anodization, the samples provided as rods of 1 cm in diameter and 3 cm in lenght, were firstly cut into 2 mm thick disks and then mechanically grinded using SiC emery paper (800-2400 grit), followed by wet polishing using diamond slurry. This was followed by sonication in acetone, ethanol and then in deionized water for 5 minutes for each one. Finally, the samples were dried with hot air and nitrogen stream.

2.1 Anodization Process

Nanoprous titania thin film was elaborated by electrochemical anodization method in a tow electrode configuration cell, Ti6Al4V alloy as a working electrode with a surface area of 0.94 cm^2 and a graphite rod with 7 mm in diameter as a counter electrode, in an electrolyte containg 0.5 wt. % Hydrofluoric acid at a constant applied potential of 10 V, provided by DC power source during 15 minutes. The distance between the tow electrodes is kept constant at 2 cm. Crystallized sample was obtained by annealing treatment of the as-anodized amorphous TiO_2 at 550 °C for 2 h.

* aghani.boucheham@gmail.com

2.2 Characterization Methods

Microstructure observation was conducted with field emission scanning electron microscopy (FE-SEM, Nova NanoSEM 430) at an operating voltage of 20 kV, the thickness of the film was evaluated on the cross-section view of the sample. Crystallographic structure of the oxide was investigated by X-ray diffraction (XRD,Philips X'PERT PRO) with Cu-Kα radiation (0.15406 nm), with a scan rate of 2°/min. The XRD profiles were compared to standards compiled by the Joint Committee on Powder Diffraction and Standards (JCPDS), with card JCPDS N°: 00-044-1294 for Ti and JCPDS N°: 00-021-1272 for TiO_2 (Anatase).

Electrochemical investigations were carried out using VMP3 research-grade multi-channel potentiostat. Electrochemical measurements were recorded using EC-Lab express software.

All electrochemical experiments were performed in 3-electrode configuration cell in 0.9 wt. % NaCl electrolyte with pH = 6.4 at room temperature. The Ti6Al4V, as-anodized and annealed titania were used as working electrode for each experiment, standard calomel reference (SCE) and platinum wire were used respectively, as reference and counter electrodes. For the open circuit potential measurements (Eocp), the potential was recorded during 1 hour, an enough duration given to allow the system to be stabilized. Electrochemical impedance spectroscopy measurements (EIS) were carried out after system stabilization at Eocp and frequencies scanning range from 100 KHz to 10 mHz for 10 frequency decades with an amplitude of ± 10 mV. The potentiodynamic polarization tets were performed by scanning the applied potential from – 1 V/ SCE to + 1,5 V/SCE with a rate of 1 mV/s.

We note that in the current work, we have chosen intentionally, low potential value and short duration in such a case to obtain only nanoporous structure thin films. But, in another incoming work, an anodization at 60 V potential and 2.5 hours' time in ethylene glycol electrolyte was carried out to elaborate nanotubes structure.

3. RESULTS AND DISCUSSION

3.1 Formation of the Nanoporous TiO_2

Fig. 1a depicts the evolution of current density during the formation of nanoporous TiO_2 thin film by electrochemical anodization on the surface of Ti6Al4V substrate in 0.5 wt. % HF containing electrolyte for 15 minutes.

The anodization process can be summerized in three steps, as shown in Fig. 2b (inset graph), the first step (indicated as I in the graph) corresponds to the formation of a thick compact oxide layer (barrier layer) characterized by a rapid drop in the current density values. This oxide layer is formed predominantly of amorphous TiO_2 as will be presented in XRD pattern in Fig. 3. The chemical reaction that can describe the step number I is as follows:

$$Ti + 2H_2O - 4e \rightarrow TiO_2 + 4H^+ \qquad (3.1.1)$$

Where: H_2O from the electrolyte and Ti from the alloy.

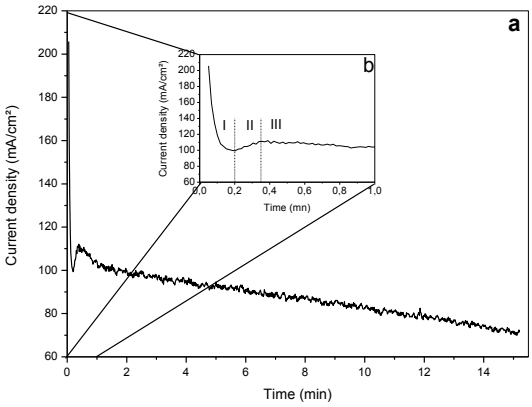

Fig. 1 – Evolution of the current density as a function of time during anodization process

In the step number II, an increase in current density values can be observed due to the breakdown of the barrier oxide layer manifested by the formation of pits on the surface of this latter caused by the presence of fluoride ions and assisted by the applied electric field. This process step can be ascribed to the following reaction:

$$TiO_2 + 6F^- + 4H^+ \rightarrow [TiF_6]^{2-} + 2H_2O \qquad (3.1.2)$$

The current density values keep relatively constant in the last step (number III) of the anodization process with the increasing of the nanopores depth.

3.2 SEM Observation

The morpholgy of the substrate surface, the as-anodized titania and anneald at 550 °C for 2 h were illustrated, respectively, in Fig. 2.

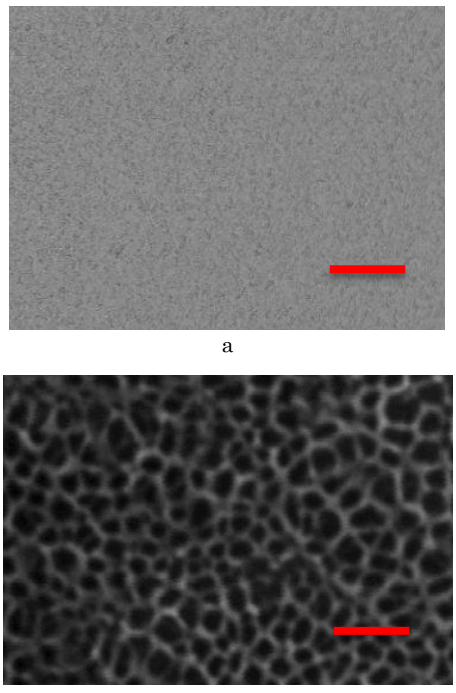

a

b

Fig. 2 – FE-SEM micrographs of Ti6Al4V alloy surface (a), as-anodized and annealed oxide (b). The scale bar is 200 nm

As can be clearly appeared in Fig. 2b, the as-anodized layer is entirely formed of nanopores witch are covered uniformly the Ti6Al4V surface alloy. No significant changes were observed on the morphology of the as-produced layer after the annealing at 550 °C for 2 h, as shown in Fig. 2b, which confirm the thermal stability of the titanium dioxide under nanoporous structure. The mean diameter of the nanopores is approximately 40 nm.

From the cross-section view of the thin film, the thickness of the as-anodized TiO_2 layer is about 200 nm. It was concluded that the nanoporous morphology is a promising characteristic for dental implants since it favors the osseointegration [22].

Anodizing aluminium can form Al_2O_3 nanopores, however the electrolyte used to anodize Al may be different as compared to the electrolyte used to anodize Ti and its alloys, this is because the chemical properties of titanium and aluminum are different. The metal that is used in this study is Ti6Al4V alloy, which is composed of 90 % Ti, 6 % Al and 4 %V. since the substrate contains majority of Ti, the predominant composition of nanopores is TiO_2, and however, having the aluminum in the alloy, there may also be some aluminum oxide present in the titania nanopores content.

3.3 Phase Composition

The X-ray diffraction patterns of the Ti6Al4V alloy, the as-made and the annealed anodic thin films, were presented in Fig. 3.

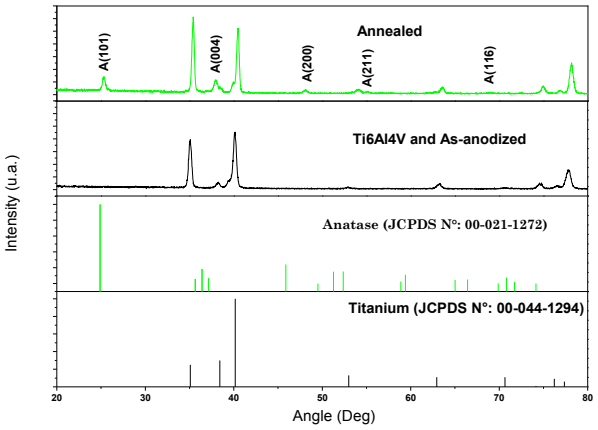

Fig. 3 – XRD patterns of Ti6Al4V alloy, as-anodized and annealed

From the corresponding XRD pattern of the as-anodized titania recorded above, it is obvious that the layer formed on the Ti6Al4V alloy surface is amorphous as reported in the literature [23] since the peaks seen correspond to the substrate pattern as referred to the titanium JCPDS N: 00-044-1294.

Anatase is the predominant phase present in the layer after the annealing at 550 °C as shown in the corresponding XRD pattern as referred to the anatase JCPDS N : 00-021-1272, in addition to the substrate peaks. Amorphous nanoporous titania formed on the surface of Ti6Al4V alloys by anodic oxidation was crystallized to anatase phase after the annealing at 550 °C in air for 2 hours.

3.4 Electrochemical Investigation

The evolution of the open circuit potentials (E_{ocp}) vs. time and the potentiodynamic polarization curves for Ti6Al4V alloy, as-anodized and annealed layers are reported in Fig. 4 and Fig. 5, respectively.

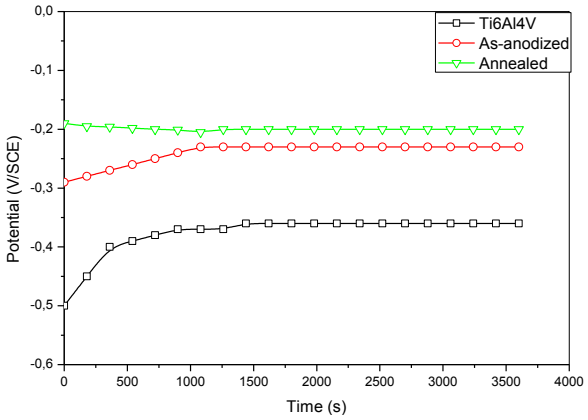

Fig. 4 – Open circuit potential vs. time for Ti6Al4V alloy, as-anodized and annealed

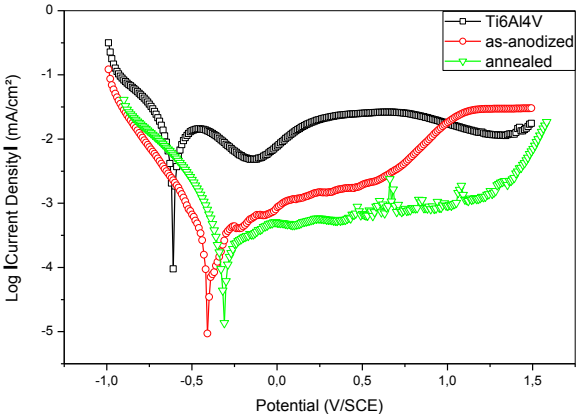

Fig. 5 – Potentiodynamic polarization curves for Ti6Al4V alloy, as-anodized and annealed

The aspect of the open circuit potential (Eoc) variation with time is an indicator for the corrossivity/passivity of the studied samples. As can be seen in Fig. 4, the corresponding plot of the smooth Ti6Al4V surface alloy exhibits a pronounced increasing from – 0.50 V/SCE towards more positive values until reaching a constant value of E_{oc} (Ti6Al4V) = – 0.35V/SCE after the stabilization. This phenomenon can be explained, as reported in [17], by the formation of a protective passive oxide film on the surface the Ti6Al4V alloy. The as-anodized corresponding OCP plot behaves slightly as the same trend as the substrate E_{oc} (as-anodized) = – 0.22 V/SCE. Contrary to what be found previously, annealed corresponding OCP variation remains stable during the one hour measurements with E_{oc} (annealed) = – 0.19 V/SCE.

On the basis of the steady-state OCP values obtained after one hour immersion in 0.9 wt. % NaCl solution, one may perform a classification of the three different studied surfaces (smooth, as-anodized and

annealed) in terms of resistance to corrosion; the more positive potential corresponds to the sample witch resists better to the degradation.

Table 1 – Corrosion potential, corrosion current densities values and Tafel slopes of Ti6Al4V alloy, as-anodized and annealed

	E_{corr} (mV)	I_{corr} (μA/cm²)	β_a (mV/Dec)	$-\beta_c$ (mV/Dec)
Ti6Al4V	– 612	3.68	302.5	302.9
As-anodize	– 371	0.152	282.5	198.3
Annealed	– 300	0.205	764.4	177

Another method used widely in dental field to assess the corrosion behavior of metallic biomaterials in saline electrolyte is potentiodynamic polarization technique. As reported in Fig. 5, the variation of the current densities with the applied potentials for the all studied samples can be divided in four distinguished domains: The first, is the cathodic domain, where the current is determined by the reduction of oxygen, it ranges from – 1 V/SCE to – 0.612 V/SCE for Ti6Al4V alloy, from – 1 V/SCE to – 0.371 V/SCE for as-anodized sample and from – 1 V/SCE to – 0.3 V/SCE for annealed sample. We note that the cathodic domain ends at the corrosion potential (E_{corr}) of each sample. The second domain consists of the transition from cathodic to anodic current at E_{corr}, where the corrosion begin to occur, it ranges from – 0.612 V/SCE to – 0.47 V/SCE for Ti6Al4V alloy, from – 0.371 V/SCE to – 0.24 V/SCE for as-anodized sample and from – 0.3 V/SCE to – 0.06 V/SCE for annealed sample. The third domain is the passive region, where a protective layer was formed on the surface of the samples, it ranges from – 0.612 V/SCE to + 0.08 V/SCE for Ti6Al4V alloy, from – 0.24 V/SCE to + 0.6 V/SCE for as-anodized sample and from – 0.06 V/SCE to + 1.26 V/SCE for annealed sample, lastly, the transpassive domain, this region manifested by the rupture of the protective layer formed previously at the passive domain, generally by pitting corrosion type [24]. L. Benea, et al. have reported the same polarization domains on the potentiodynamic polarization curves of untreated and electrochemical modified Ti6Al4V alloy in bio-simulated Fusayama-Mayer saliva [17].

Shifting in Ecorr values towards noble potentials was remarkably observed, indicating the improvement of the corrosion resistance due to the modification of the morphology and the structure of the surfaces, this finding corroborates the obtained results of the open circuit potentials. Other electrochemical parameters for the studied samples are summarized in Table 1 as extrapolated from Tafel plots.

In order to deepen our study on the corrosion properties, the electrochemical impedance spectroscopy technique was performed. Fig. 6 and Fig. 7 depict, respectively, the Nyquist diagrams with the equivalent electrical circuits (inset graphs) and the Bode plots for Ti6Al4V alloy, as-anodized and annealed titania layer under open circuit potential conditions in 0.9 wt. % NaCl solution.

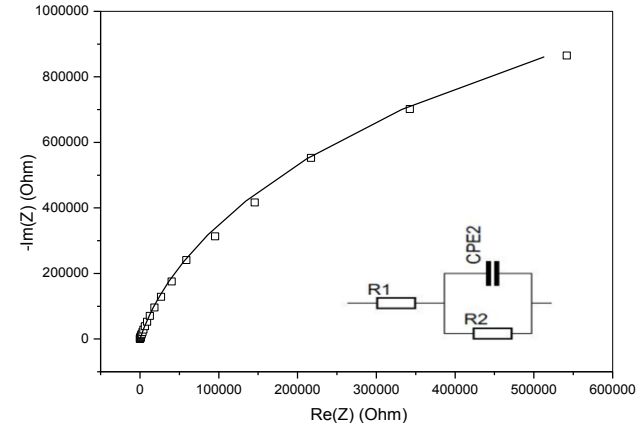

a

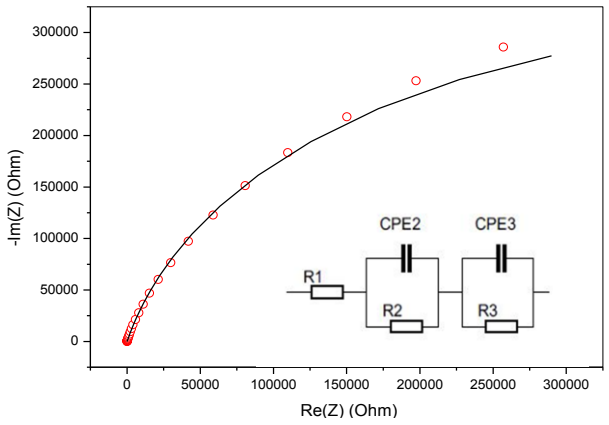

b

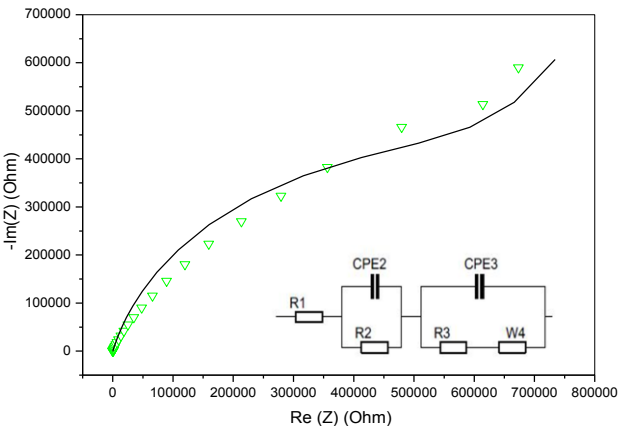

c

Fig. 6 – Nyquist diagrams and Randles equivalent electrical circuit (inset graphs) for Ti6Al4V alloy (a), as-anodized (b) and annealed (c). Symbols represent experimental data, lines represent the fitted data

The Nyquist diagram illustrated in Fig. 6a for Ti6Al4V alloy exhibits a single depressed semicircle loop which corresponds to one constant phase element (CPE2), while, two superposed semicircle loops can be observed at high frequencies and middle-low frequencies in the Nyquist diagrams for the as-anodized and the annealed layer reported in Fig. 6b and Fig. 6c, respectively, which correspond to two constant phase elements (CPE2, CPE3), for the latter one, it comprises

Table 2 – EIS equivalent Randle circuit parameters

	R_1 (Ω)	CPE_2 ($F.s(a^{-1})$)	a_2	R_2(Ω)	CPE_3($F.s(a^{-1})$)	a_3	R_3(Ω)	W_4 ($Ω.s^{-1/2}$)
Ti6Al4V	45.65	$20.42e^{-6}$	0.91	2.53e6				
As-nodized	80.81	$24.75e^{-6}$	0.86	350916	$53.51e^{-6}$	0.81	647752	
Annealed	60.56	13e-6	0.84	768419	0.16e-3	0.56	2.60 e6	114574

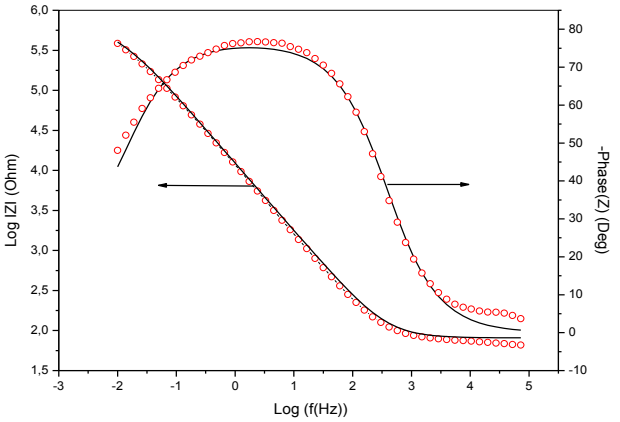

Fig. 7 – Bode plots for as-anodized sample. Symbols represent experimental data, lines represent the fitted data

also of a sloping line corresponding to Warburg element (W4). The impedance data are fitted to the equivalent electrical circuits (EEC), as represented in fig.6 (inset graphs). The elements of the EEC proposed are: R_1 for solution resistance, R_2 for charge transfer resistance of the passive film in the case of the Ti6Al4V alloy and charge transfer resistance of the nanoporous layers for the as-anodized and the annealed samples, CPE_2 for constant phase element of the double layer, CPE_3 for the inner compact oxide for the as-anodized and the annealed samples, R_3 for charge transfer resistance, W_4 related to the mass transport limitation by diffusion [15]. J. Grotberg, et al. have reported similar equivalent electrical circuits when they perform the EIS on the Ti6Al4V, as-anodized and annealed nanotubes under OCP conditions in solution containing proteins [15]. Table 2 recapitulates the obtained values of each element as calculated by EC-Lab express software from the fit of the experimental data.

The Bode plots represented in Fig. 7 corroborate exactly the earlier findings. It is noted that the polarization resistance (R_p), extracted from equivalent electrical circuits which corresponds to the sum of R_2 and R_3, is proportional to the resistance to corrosion, R_p (annealed) = $1{,}3.10^7$ Ω > R_p (as-anodized) = $0{,}99.10^7$ Ω > Rp (Ti6Al4V alloy) = $2{,}53.10^6$ Ω, that's confirm the resistance corrosion of the annealed layer compared with the as-anodized and the Ti6Al4V alloy.

4. CONCLUSION

Amorphous nanoporous titania layers were elaborated on the surface of Ti6Al4V medical grade alloy by electrochemical anodization in aqueous solution containing fluoride ions (F^-).

The crystallization of the as-anodized TiO_2 to anatase phase was carried out at an annealing temperature of 550 °C for 2 hours. Both the amorphous and the crystallized structures of the titania layers enhance the electrochemical behavior of the Ti6Al4V alloy by shifting the open circuit potentials and the corrosion potentials towards most noble values.

The Ti6Al4V alloys coated with anodic nanoporous titania thin films can be successfully employed for dental application as implants.

ACKNOWLEDGEMENTS

This work was supported by the Fond National à la recherche, DG-RSDT- Algeria. The anodization processes and the electrochemical measurements were performed at Centre de Recherche en Technologie des Semi-conducteurs pour l'Energetique (CRTSE, Algiers) with the agreement of its director. FE-SEM observations were carried out at METU GUNAM, Turkey by Miss Yasmina Keriti. The medical grade Ti6Al4V alloys used in this work were provided free of charge by Implant Dokum Company- Turkey. They are all gratefully acknowledged.

REFERENCES

1. M. Kalisz, M. Grobelny, M. Mazur, M. Zdrojek, D. Wojcieszak, M. Świniarski, J. Judek, D. Kaczmarek, *Thin Solid Films* **589** No 31, 356 (2015).
2. Dong Bok Lee, Iryna Pohrelyuk, OlehYaskiv, Jae Chun Lee, *Nanoscale Res. Lett.* 7:21 (2012).
3. B. Bozzini, P. Carlino, L. D'Urzo, V. Pepe, C. Mele, F. Venturo, *J. Mater. Sci.: Mater. Med.* **19**, 3443 (2008).
4. Júlio C.M. Souza, Sandra L. Barbosa, Edith A. Ariza, Mariana Henriques, Wim Teughels, Pierre Ponthiaux , Jean-Pierre Celis, Luis A. Rocha, *Mat. Sci. Eng. C* **47**, 384 (2015).
5. M.Yu. Gazizova, M.B. Ivanov, T.N. Vershinina, *J. Nano-Electron. Phys.* **7** No 4, 04081 (2015).
6. C. Vitelaru, N. Ghiban, A.C. Parau, M. Balaceanu, F. Miculescu, A. Vladescu, *Mat. Sci. Eng. Tech.* **45** No 2, 91 (2014).
7. Naoya Masahashi, Yoshiteru Mizukoshi, Satoshi Semboshi, Kazuyo Ohmura, Shuji Hanada, *Thin Solid Films* **520** No 15, 4956 (2012).
8. Si-Eun Kim, Sang-Bae Lee, Jeong-Jong Park, Kwang-Mahn Kim, Kyoung-Nam Kim, *Surf. Interface Anal.* **42** No 6, 524 (2010).
9. Yardnapar Parcharoen, Puangrat Kajitvichyanukul, Sirinrath Sirivisoot, Preecha Termsuksawad, *Appl. Surf. Sci.* **331**, 54 (2014).
10. Song Wang, Zhenhua Liao, Yuhong Liu, Weiqiang Liu, *Surf. Coat. Tech.* **240**, 470 (2014).
11. Song Wang, Yuhong Liu, Caixia Zhang, Zhenhua Liao, Weiqiang Liu, *Tribol. Int.* **79**, 174 (2014).
12. K.M. Deen, A. Farooq, M.A. Raza, W. Haider, *Electrochim.*

Acta. **117**, 329 (2014).
13. A.R. Rafieerad, A.R. Bushroa, E. Zalnezhad, M. Sarraf, W.J. Basirun, S. Baradaran, B. Nasiri-Tabrizi, *Ceram. Int.* **41** No 9 part A, 10844 (2015).
14. L.N. Inasaridze, A.V. Balmasov, *Pro. Met. Phys. Chem. Surf.* **51** No 4, 523 (2015).
15. John Grotberg, Azhang Hamlekhan, Arman Butt, Sweetu Patel, Dmitry Oyhman, Tolou Shokuhfar, Cortino Sukotjo, Christos Takoudis, Mathew T. Mathew, *Mat. Sci. Eng. C* **59**, 677 (2015).
16. Lidia Benea, Eliza Danaila, Pierre Ponthiaux, *Corros. Sci.* **91**, 262 (2015).
17. Lidia Benea, Eliza Mardare-Danaila, Marilena Mardare, Jean-Pierre Celis, *Corros. Sci.* **80**, 331 (2014).
18. A. Vladescu, M. Braic, F. Ak Azem, I. Titorencu, V. Braic, V. Prunac, A. Kiss, A.C. Paraub, I. Birlik, *Appl. Surf. Sci.* **354** Part B, 373 (2015).
19. Yingmin Su, Satoshi Komasa, Tohru Sekino, Hiroshi Nishizaki, Joji Okazaki, *Mat. Sci. Eng. C* **59**, 617 (2016).
20. Yingmin Su, Satoshi Komasa, Tohru Sekino, Hiroshi Nishizaki, Joji Okazaki, *J. Nanomater.* **2015**, ID 358951 (2015).
21. J.M. Hernández-López, A. Conde, J.J. de Damborenea, M.A. Arenas, *RSC Adv.* **4**, 62576 (2014).
22. Laís T. Duarte, Sonia R. Biaggio, Romeu C. Rocha-Filho, Nerilso Bocchi, *Corros. Sci.* **72**, 35 (2013).
23. M. Kulkarni, A. Mazare, E. Gongadze, Š. Perutkova, V. Kralj-Iglič, I. Milošev, P. Schmuki, A. Iglič, M. Mozetič, *Nanotechnology* **26**, 062002 (2015).
24. Xuanyong Liu, Paul K. Chub, Chuanxian Dinga, *Mat. Sci. Eng. R* **47** No 3, 49 (2004).